The Astrophysical Journal, 974:289 (11pp), 2024 October 20 https://doi.org/10.3847/1538-4357/ad71cc
© 2024. The Author(s). Published by the American Astronomical Society.
OPEN ACCESS

Measurements of Magnetic Cloud Expansion through Multiple Spacecraft in Radial Conjunction

Wenyuan Yu, Nada Al-Haddad, Charles J. Farrugia, Noé Lugaz, Bin Zhuang, Florian Regnault, and Antoinette B. Galvin
University of New Hampshire, Durham, NH, USA
Received 2024 April 29; revised 2024 August 6; accepted 2024 August 19; published 2024 October 17

Abstract

The aim of this study is to use multispacecraft measurements of interplanetary magnetic clouds (MCs) to better constrain and understand the effect of expansion on their magnetic field properties. We develop a parameter (γ) for comparing magnetic field components measured at multiple spacecraft. We use the minimum variance technique on the magnetic field data to obtain the axial and azimuthal components. The parameter γ acts at the front boundary as a measure of the global difference in the evolution with heliospheric distance of the axial and azimuthal magnetic field components of MCs. Our goal is to determine whether the studied MCs exhibit self-similar expansion and, if so, whether this expansion is predominantly isotropic or radial, based on the estimated γ. Through our analysis of data from multiple spacecraft, we observe a notable consistency in the γ values across the examples examined. We find that the overall expansion of these MCs tends to be isotropic, while the local expansion of MCs, derived from the γ values measured at the rear boundary of MCs, usually shows anisotropic behavior, particularly when the distances between the observations from the two spacecraft are relatively short. This discovery offers insights for refining flux rope models and advancing our comprehension of the expansion processes associated with coronal mass ejections.

Unified Astronomy Thesaurus concepts: Solar physics (1476); Solar wind (1534); Solar magnetic fields (1503)

1. Introduction

Magnetic clouds (MCs; L. Burlaga et al. 1981) are very important interplanetary structures that form a subset of the interplanetary coronal mass ejections (ICMEs). The MC/ICME occurrence ratio is found to be about 15% at solar maximum and almost 100% at solar minimum (H. V. Cane & I. G. Richardson 2003; Y. Chi et al. 2016). MCs are defined by an enhanced magnetic field strength with a smooth rotation of the magnetic field vector in a plasma of low proton temperature or beta. It was noticed early on that MCs expand as they propagate away from the Sun (L. Burlaga et al. 1981; L. W. Klein & L. F. Burlaga 1982), as seen by a clear decreasing trend in all or most of the proton bulk velocity profile in the in situ measurements. In particular, the radial expansion of MCs also shows a clear decrease of the magnetic field strength and an increase of the size of the structure's cross section (Y. Liu et al. 2005; E. E. Davies et al. 2021).

MCs are often thought to be twisted magnetic flux rope structures (L. Burlaga et al. 1981). Observations by a single spacecraft provide only measurements of a time series of coronal mass ejection (CME) parameters, which can be traditionally analyzed as 1D cuts. Therefore, analytical or numerical flux rope models are necessary to infer their 3D structure (P. Démoulin et al. 2008). Most analytical flux rope models are based on the principles of magnetohydrodynamics (MHD), which describe the behavior of the magnetic fields in a plasma considered as a fluid. The models usually assume that the magnetic fields within the flux rope are force-free (magnetic tension force is balanced by the pressure gradient force). Such are the popular Lundquist models (constant α parameter in the magnetic field solutions) and the Gold–Hoyle models (constant twist value in the solutions) (S. Lundquist 1950; T. Gold & F. Hoyle 1960; L. F. Burlaga 1988; R. P. Lepping et al. 1990; C. J. Farrugia et al. 1999; B. Vršnak et al. 2019), as well as other non-force-free models, like M. A. Hidalgo et al. (2002; constant current densities in the solutions). These models are simple and widely used in the scientific community. The models reconstruct these flux rope structures and output the shape, size, and other properties (which could not be measured directly from the observation but can be derived from the MHD equations). They also can be used to further study the dynamics of MCs with multispacecraft observations, including their propagation and interaction with the solar wind (V. A. Osherovich et al. 1993; B. Vršnak et al. 2004; E. E. Davies et al. 2022; B. Zhuang et al. 2023). As the flux ropes propagate, expansion plays a critical role in their evolution. MCs expand either (i) because they have a stronger internal (mainly magnetic) pressure than the surrounding solar wind or (ii) because the pressure of the surrounding solar wind falls faster with increasing distance from the Sun than the pressure inside the flux rope. Inside 0.5 au, the first factor is thought to be the main cause, but outside 0.5 au, the second is the preferred scenario, causing flux ropes to expand into the interplanetary medium (A. M. Gulisano et al. 2010; N. Lugaz et al. 2020). As the flux rope expands, the magnetic field strength decreases, which reduces the tension forces that hold the flux rope together (P. Démoulin & S. Dasso 2009). This can cause the flux rope to become unstable and potentially break apart.

While single-spacecraft measurements can only provide information on the local expansion of the MC at a specific point, multispacecraft measurements can help us analyze the global expansion by measuring the same MC at different locations as long as the distances between these observations are larger than the size of the MC (for a discussion of the effects of smaller separations, see F. Regnault et al. 2023, 2024). In specific studies, the expansion of MCs has been found to be close to self-similar by using multispacecraft observations

Original content from this work may be used under the terms of the Creative Commons Attribution 4.0 licence. Any further distribution of this work must maintain attribution to the author(s) and the title of the work, journal citation and DOI.

(P. Démoulin & S. Dasso 2009; S. W. Good et al. 2019); that is, the magnetic field strength decreases with heliocentric distance. For example, E. E. Davies et al. (2022) derive that the mean magnetic field strengths decrease with distances as $B_{\mathrm{mean}(\leqslant 1\ \mathrm{au})} \propto r^{-1.49\pm1.12}$ and $B_{\mathrm{mean}(\geqslant 1\ \mathrm{au})} \propto r^{-1.29\pm0.83}$, respectively. In these studies (E. E. Davies et al. 2021, 2022), the authors compare the total magnetic field magnitudes of different CMEs observed by spacecraft at different locations, and they arrive at the conclusion that the expansion of MCs is not self-similar or cylindrically symmetric. Interestingly, while these works focus on studying the evolution of the magnetic field magnitude with distance, there are very few works studying the relationship between the individual magnetic field components during the MC propagation. As such, the key science questions are (i) knowing whether, under global self-similar expansion, the magnetic field components decrease isotropically or not and (ii) knowing, under a global non-self-similar expansion, what the relationship is between the magnetic field components. Here, we propose to study the evolution of the magnetic field components during the MC propagation and define a parameter (γ) that can reflect the difference (or ratio) of the components (isotropic or anisotropic) by using two spacecraft observations.

Global self-similar expansion is usually assumed when deriving the analytical expanding models, for example, the expanding Lundquist model (C. J. Farrugia et al. 1992, 1993; H. Shimazu & M. Vandas 2002; Y. Wang et al. 2015) and the expanding Gold–Hoyle model (Y. Wang et al. 2016). The expanding Lundquist model was first proposed by C. J. Farrugia et al. (1992), and the expansion was assumed to be self-similar and radial. In this case, the toroidal magnetic field component B_z decreases faster than the poloidal component based on $B_\phi = (B_0/\tau)J_1(\alpha r/\tau)$ and $B_z = (B_0/\tau^2)J_0(\alpha r/\tau)$. Here, the parameter τ is defined as $\tau = 1 + t/t_0$, where t_0 is the duration that the MC structure has been expanding self-similarly before it encounters the spacecraft. J_0 and J_1 are Bessel functions of order 0 and 1. It was found that the expansion in the radial direction introduces an asymmetry in the total magnetic field profile in in situ measurements: the magnetic field strength peaks toward the front and not at the center, as it does in the static case. This asymmetry may be caused by the global expansion (V. A. Osherovich et al. 1993; F. Regnault et al. 2023).

H. Shimazu & M. Vandas (2002) and D. B. Berdichevsky et al. (2003) developed another self-similar, expanding Lundquist model, this time for an isotropic expansion of the flux rope structure. Under this assumption, it was found that the toroidal and poloidal magnetic field components decrease at the same rate. In the solutions, the poloidal magnetic field component $B_\phi = (B_0/\tau^2)J_1(\alpha r/\tau)$, and the toroidal component $B_z = (B_0/\tau^2)J_0(\alpha r/\tau)$. The parameters used in these equations are the same as in the radial expansion Lundquist model.

The main difference between these two (i.e., radially or isotropically) expanding solutions mentioned above (C. J. Farrugia et al. 1992; H. Shimazu & M. Vandas 2002) is the behavior of the azimuthal component B_ϕ. It is, however, difficult to determine if B_ϕ decreases slower than B_z during the propagation and expansion process of the flux rope with observations from only a single spacecraft. Therefore, observations of the same MC from multiple spacecraft at different distances from the Sun can help provide more information about how the expansion of the MC varies with distance. This result provides useful information to refine the expanding models and better understand the dynamics of magnetic flux ropes.

Analyzing multispacecraft observations is an approach used in space physics research that involves aligned observations of solar transients from multiple spacecraft at different locations in space (M. Leitner et al. 2007; B. Vršnak et al. 2019; T. M. Salman et al. 2020; E. E. Davies et al. 2021, 2022). By combining data from multiple spacecraft, researchers can obtain detailed information about the spatial and temporal evolution of a given phenomenon, here expansion (S. W. Good et al. 2019; N. Lugaz et al. 2020). The local measurements of the bulk velocity profile provide information on the local expansion. Multispacecraft observations provide us data to analyze the global expansion by checking the decrease of the magnetic field strength during propagation. We note that N. Lugaz et al. (2020) find that the radial expansion is inconsistent between local and global measurements, but this study focused primarily on the innermost heliosphere, i.e., distances below 1 au, where the CME may be expected to not yet be in force balance. Our focus here is to find out what type of expansion MCs undergo during propagation away from the Sun by checking the variation with distance of the magnetic field components, i.e., whether it is radially or isotropically self-similar or, indeed, if it is self-similar at all.

The rest of the paper is organized as follows. In Section 2, we describe the methodology used in this study and present the selected events observed by multiple spacecraft. In Section 3, we present detailed analyses of three MC cases observed by two spacecraft and show the fitting results by the radial or isotropic expanding Lundquist solutions mentioned above. In Section 4, we discuss the results and conclude.

2. Methodology

2.1. Definition of the Parameter Gamma

In our work, we use the multispacecraft in situ measurement approach to enhance our understanding of MC expansion. Particular attention is given to the evolution of the components (axial and azimuthal) of the MC's magnetic field. Since the measurements cannot directly provide us the toroidal and poloidal magnetic field components, we use the minimum variance analysis (MVA) on the magnetic field components observed in the geocentric solar ecliptic (GSE) or radial–tangential–normal (RTN) coordinate systems (B. U. Ö. Sonnerup & M. Scheible 1998). The MVA outputs eigenvectors: the eigenvector associated with the intermediate eigenvalue is the direction of the MC axis, and the eigenvector associated with the maximum eigenvalue is related to the azimuthal component of the magnetic field. We then use the above eigenvectors to transform the magnetic field components in the GSE or RTN coordinate systems to the MVA coordinates.

To describe the type of expansion, we introduce a parameter "gamma," γ. γ is defined as $\gamma = \frac{B_{z2}/B_{z1}}{B_{\phi2}/B_{\phi1}}$ based on the in situ magnetic field measurements made at two different heliocentric distances. In the ideal circular cross-section cylinder flux rope structure, B_z is along the axis of the MC (toroidal component), and B_ϕ is the azimuthal magnetic field component (poloidal component). Here, B_{z1} and $B_{\phi1}$ are the axial and azimuthal magnetic field components at the first spacecraft (SC) obtained by using the MVA method. Similarly, B_{z2} and $B_{\phi2}$ are magnetic field components at the second SC. The γ parameter determines if the axial magnetic field component B_z decreases at the same rate as or faster than the azimuthal magnetic field component B_ϕ. When the two magnetic field components (B_ϕ and B_z)

Table 1
Nine MC Conjunction Events Observed by Multiple Spacecraft

No.	SC1	Date and Time	SC2	Date and Time	ΔΦ	MVA Ratio	MVA Axis	γ
1	Helios 1	1978-03-02T00:00:00–	Voyager 2	1978-03-07T02:30:00–	−13	16.5	(−49.3, 119)	1.08
	(0.85 au)	1978-03-03T05:45:00	(2.5 au)	1978-03-09T04:00:00		21.8	(−29.9, 87.7)	0.921
2	ACE	2000-07-15T19:30:00–	NEAR	2000-07-17T01:00:00–	1.9	6.7	(32.2, 58.4)	1.19
	(0.99 au)	2000-07-16T12:30:00	(1.76 au)	2000-07-18T10:00:00		9.81	(58, 28.4)	1.38
3	MES	2009-02-15T04:24:00–	STB	2009-02-18T18:42:00–	1	9.58	(31, 54.1)	1.06
	(0.326 au)	2009-02-15T19:00:00	(1 au)	2009-02-19T17:00:00		2.69	(10.8, 131)	1.4
4	MES	2010-11-05T16:30:00–	STB	2010-11-08T03:00:00–	0.2	12.7	(46.5, 108)	0.913
	(0.47 au)	2010-11-06T14:00:00	(1.08 au)	2010-11-09T09:00:00		43.2	(23, 89.8)	0.565
5	MES	2011-11-05T00:43:00–	STB	2011-11-06T22:57:00–	−4.8	4.09	(5.92, 83.3)	1.24
	(0.44 au)	2011-11-05T17:05:00	(1.09 au)	2011-11-08T17:48:00		4.16	(5.95, 126)	1.15
6	STB	2012-05-08T18:38:00–	Juno	2012-05-13T15:43:00–	7.24	3.47	(−45.3, 104)	0.591
	(1 au)	2012-05-09T00:36:00	(2.13 au)	2012-05-14T07:43:00		3.12	(−19.4, 157)	0.636
7	STA	2012-11-14T10:44:00–	Juno	2012-11-19T17:00:00–	−18.34	3.53	(36, 95.6)	1.26
	(0.97 au)	2012-11-15T13:47:00	(2.19 au)	2012-11-21T01:00:00		13.9	(−25.9, 125)	0.874
8	Wind	2013-04-14T16:30:00–	Juno	2013-04-17T01:30:00–	1.01	3.91	(−64.2, 2.3)	1.26
	(0.99 au)	2013-04-15T18:00:00	(1.63 au)	2013-04-18T13:00:00		4.02	(−70, 23.4)	0.932
9	MES	2014-02-17T07:03:00–	ACE	2014-02-19T12:00:00–	4.8	11.4	(41.2, 31.1)	0.958
	(0.35 au)	2014-02-17T09:00:00	(1 au)	2014-02-20T02:35:00		4.72	(50.8, 111)	1.33

Note. The columns show multiple SCs, the MC's start and end date and time at the two SCs, their distances away from the Sun (au), the difference in longitude between the two SCs (degrees), the MVA eigenvalue ratio (medium/minimum) and related axis orientations (θ, ϕ; degrees), and the $\gamma_{\rm front}$ and $\gamma_{\rm rear}$ values.

decrease at the same rate, the MC undergoes isotropic expansion ($\gamma = 1$). When the two magnetic field components do not decrease at the same rate ($\gamma \neq 1$), the MC undergoes anisotropic expansion. Especially when $\gamma < 1$, the axial component expands faster than the azimuthal components. When it is small enough, the expansion tends to be radial.

Parameters $\gamma_{\rm front}$ and $\gamma_{\rm rear}$ are the two values related to the expansion at the front-half part or rear-half part (in which $B_{\phi 1}$ and $B_{\phi 2}$ are related maximum absolute values around the front or rear boundaries and B_{z1} and B_{z2} are maximum absolute values close to the center when B_ϕ changes sign). When the MC passes over the spacecraft, the front boundary of the MC has not been affected by the observation (aging; see F. Regnault et al. 2023) and the MC local expansion. Therefore, $\gamma_{\rm front}$ only presents the effect of the global expansion. On the other hand, $\gamma_{\rm rear}$ reflects the effects of both global expansion (MC's external expansion) and local expansion, as well as other effects.

2.2. Event Selection

In this paper, we analyze in situ measurements from multiple spacecraft to study the expansion effect on the MC magnetic fields. Magnetic field data are from magnetometers on board ACE, Helios, Juno, MESSENGER, NEAR, STEREO, Voyager, and Wind. The field data we use are at 1 minute resolution except for MESSENGER's data, which are at 0.05 s resolution. We obtain the magnetic field data from CDAWeb[1] for the events observed by ACE, Helios, MESSENGER, STEREO, Voyager, and Wind, and Planetary Plasma Interactions[2] for the ones observed by the Juno and NEAR spacecraft.

We select the events that were observed by at least two spacecraft separated by $<20°$ in longitude but >0.5 au in the radial direction. While the average size of MCs at 1 au is about 0.2 au (R. P. Lepping et al. 1990), the large radial separation we chose (>0.5 au) distinguishes the effects of global from local expansion and should give reliable results. We use the published MC list measured by multiple spacecraft (T. Mulligan et al. 2001; M. Leitner et al. 2007; T. M. Salman et al. 2020; E. E. Davies et al. 2022). We require that the MCs observed by two spacecraft have clear rotations in the magnetic field vector. If velocity data observed at the spacecraft are available, we prefer the events that show a clear expanding structure in all or most of the MCs, as seen by a decrease in the time profile of the bulk speed. We then use the MVA method (B. U. Ö. Sonnerup & M. Scheible 1998) on the observed magnetic field components (in GSE or RTN coordinate systems), and then the three eigenvalues and eigenvectors are obtained. We require that the intermediate-to-minimum eigenvalue ratio be larger than 3 to ensure that the flux rope rotations are clear and the eigenvectors are well determined.

We then transfer the field components to the MVA coordinate system by using the three eigenvectors. We compare the B_z and B_ϕ measured by these two spacecraft and only keep the events that have clear maximum values in the $\boldsymbol{B}$ components.

Following these criteria, we come up with nine events observed by at least two spacecraft as listed in Table 1. We present in the table the names of the SCs, the MC's start and end date and time at the two SCs, their distances away from the Sun (in au), the difference in longitude between the two SCs (in degrees), the MVA eigenvalue ratio and related axis orientations, and the $\gamma_{\rm front}$ and $\gamma_{\rm rear}$ values.

[1] cdaweb.gsfc.nasa.gov
[2] pds-ppi.igpp.ucla.edu

2.3. MVA Results

We put these nine events into two classes by comparing the magnetic field components. For quality 1 events, the MVA is consistent between the two spacecraft; the MVA results do not show such good consistency between the two spacecraft for quality 2 events. Five events are classified as quality 1 events (E1, E2, E4, E5, and E8), and the other four events are classified as quality 2 events (E3, E6, E7, and E9). The total $\boldsymbol{B}$ and related components are plotted in Figure 1. The panels show from top to bottom the total magnetic field B_ϕ and B_z components derived from MVA, while the x-axis is the normalized time ([0, 1]). In the magnetic field panels, the red lines show SC1 results, while the blue lines present SC2 results with the second y-axis.

We then study the variation of the MCs' maximum magnetic field strength and toroidal B_z and poloidal component B_ϕ magnetic field components as a function of heliocentric distance. We compare the $\log(B_{\max})$ versus $\log(r)$, which is presented in Figure 2(a). These distributions provide the global expansion of these MCs observed by multiple spacecraft. We perform power-law fits on all of the data set, following the method described in the study of N. Lugaz et al. (2020). The maximum magnetic field strength has a functional relationship of $B_{\max} \propto r^{-1.73\pm0.39}$, while B_z has a -1.64 ± 0.405 index and B_ϕ has a -1.79 ± 0.424 and -1.82 ± 0.687 index at the front and rear boundaries separately (see Figure 2). The fitted exponential indices of B_z are the same as those of M. Leitner et al.'s (2007) result, who had a -1.64 index over modeled values. And under the self-similar expansion, the maximum magnetic field strength decreases as r^{-2} globally (E. E. Davies et al. 2022). This indicates that the B_ϕ of the MCs in this study undergo a self-similar expansion during their propagation (that is, their magnitudes are decreasing on the order of r^{-2}). The expansion of B_z is inconsistent with B_ϕ, while B_ϕ is also inconsistent at the two half-parts (front and rear). The expansion of B_ϕ at the rear part is faster than the front part (Figures 2(c) and (d)).

3. Case Studies

We now present three case studies by using our method of checking the γ values to figure out if the MC undergoes isotropic or radial self-similar expansion. We also use the expanding Lundquist models (both radial expanding and isotropic expanding solutions) to fit the three $\boldsymbol{B}$ components and check which solution fit the observations better, similar to our work in W. Yu et al. (2022). The details of the fitting are given in Table 2. We use "F" to indicate the fitting results from C. J. Farrugia et al.'s (1992) radially expanding Lundquist model and "V" to indicate the results from H. Shimazu & M. Vandas's (2002) isotropically expanding Lundquist model. In Table 2, we present the latitude (θ; degrees) and longitude (ϕ; degrees) angles of the flux rope axis, the impact parameter (IP), the radius (R; au), the magnetic field magnitude at the axis (B_0; nT), the helicity (H, ±1), $\alpha \times R/\tau$ at the rear boundary, the expansion time before the MC encounters the SC (t_0; hr), the normalized chi-square of the three B components (χ^2), the normalized chi-square of the total magnetic field ($\chi^2_{B_{\text{total}}}$), the normalized chi-square of the total magnetic field of the front part of the MC (dividing the MC by the peak of the B_{total}), and the normalized chi-square of the total magnetic field of the rear part of it.

3.1. MC1—Measured by Helios 1 and Voyager 2 on 1978 March 2–9

The first MC example (E1) was measured by the Helios 1 and Voyager 2 spacecraft in the year 1978. The magnetic fields are plotted in Figure 1(a). The fitting results are presented in Figure 3. The start and end times of the MC observed by Helios 1 are 1978-03-02T00:00:00–1978-03-03T05:45:00, and those of Voyager 2 are 1978-03-07T02:30:00–1978-03-09T04:00:00. The panels are as follows: the total $\boldsymbol{B}$ (black, observed; red, radial self-similar expansion solution; blue, isotropic self-similar expansion solution; nT), three $\boldsymbol{B}$ components in the RTN coordinate system (nT), and proton velocities (black, observed data; red, linear fitting of V_p; km s^{-1}). On the left are the results of SC1, and on the right are SC2. The first SC (Helios 1) is at 0.85 au, and the second SC (Voyager 2) is at 2.5 au. These two SCs are approximately radially aligned, with a longitude separation of $\sim13°$. This event was previously reported in M. Leitner et al. (2007) and studied in A. M. Gulisano et al. (2010). We apply the MVA method on the magnetic field components and obtain the orientation angles of the MC axis, and their longitude separation is $\sim31°$. The latitude angle separation of the axes observed by the two SCs are 19°. The eigenvalue ratios of this event are 16.5 and 21.8, which show very clear magnetic field rotations observed at the two SCs. With these large ratios, the derived B_z and B_ϕ profiles are reliable.

The peaks of the total magnetic field magnitude (B_{total}) are both in the front half of the MC, but the peak at SC2 is much closer to the center of the MC's duration. Thus, B_{total} becomes more symmetric during the propagation of this. The maximum of B_{total} has clearly decreased (28 versus 6 nT) due to the expansion. The MVA results of event 1 are shown in Figure 1(a). The B_ϕ are presented in the second panel. Both SCs observed B_ϕ to change from negative to positive. The absolute values reach maximum around the two boundaries and minimum, which is very close to zero, near the center of the MC duration. The B_z at the two SCs are presented in the third panel of Figure 1(a). They show clear rotations with peaks around the center and approach zero at the two boundaries. In this event, $\gamma_{\text{front}} = 1.08$ and $\gamma_{\text{rear}} = 0.921$. The $\gamma_{\text{front}} = 1.08$ presents the global expansion and shows that this MC undergoes isotropic self-similar expansion during its propagation in the solar wind. This means that although the magnetic field magnitude decreases by a factor of 4.7, the ratio of poloidal to axial field is more or less the same at the two spacecraft, indicating that both components decrease similarly with distance.

Figure 3 gives the fitting results at the two spacecraft. Comparing the fitting results with the observed data, both fitting qualities are close and good on the magnetic field components. However, their B_{total} show clear difference at the front-half part. The fittings at the rear-half part are better, especially the isotropic Lundquist solution, which arrives at a close result at the rear boundary. Comparing the normalized χ^2 values (0.212 versus 0.015 and 0.007 versus 0.006), the isotropic Lundquist solution also shows a better fitting on B_{total}. The fitting results argue that this MC is both globally and locally isotropically expanding.

The bulk velocity distributions at the two spacecraft are shown in the bottom panels of Figure 3. Both observations show a significant decrease, $\Delta V_p > 100$ km s^{-1}. We fit the V_p profile with equation $V_p = (V_c + r_0/t_0)/(1 + t/t_0)$. The fitted lines are also plotted in the figure (red dashed lines). The output

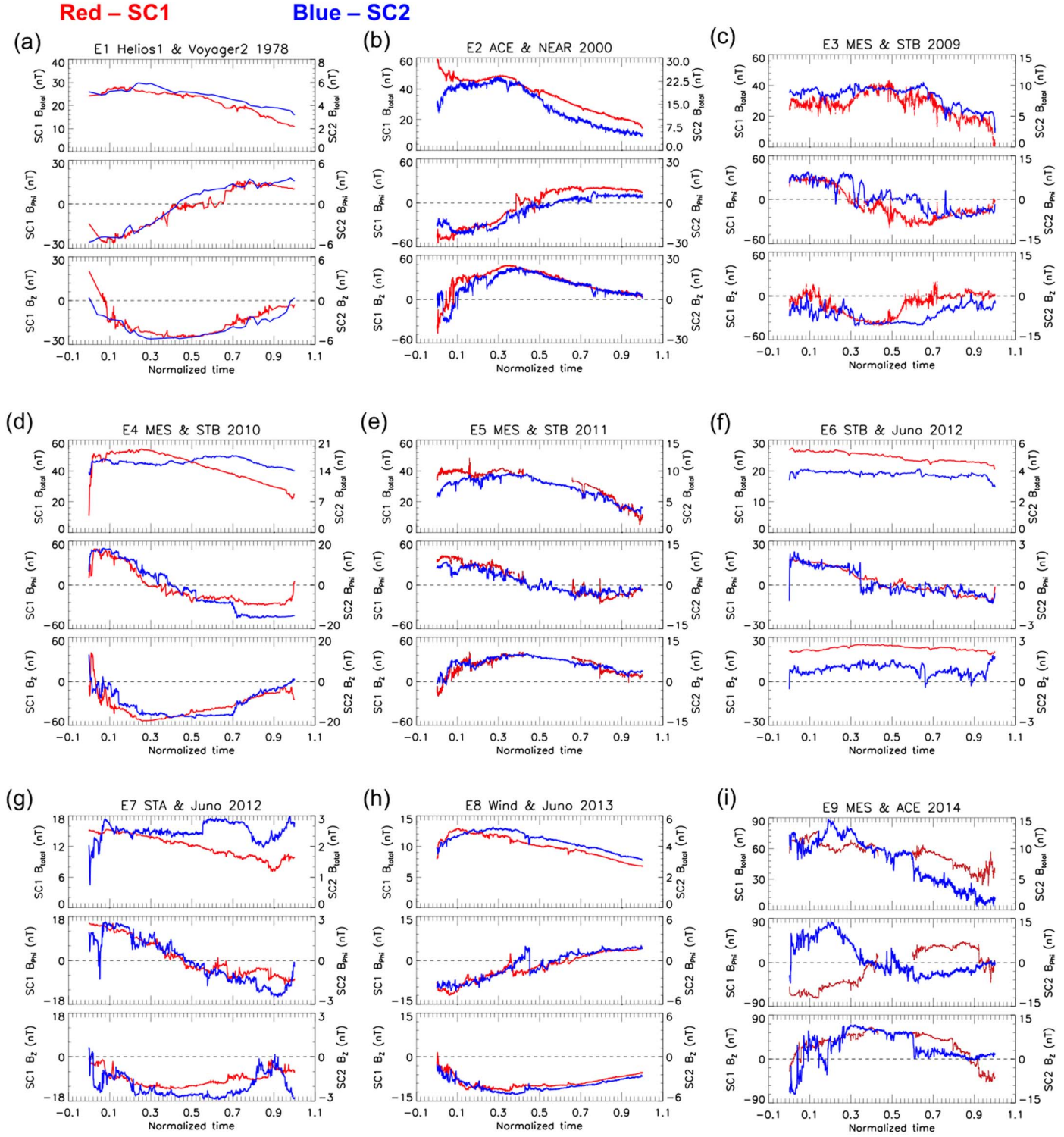

Figure 1. Nine MCs observed by multiple spacecraft. (a) MC1 observed by Helios 1 and Voyager 2 in year 1978; (b) MC2 observed by ACE and NEAR in year 2000; (c) MC3 observed by MESSENGER and STB in year 2009; (d) MC4 observed by MESSENGER and STB in year 2010; (e) MC5 observed by MESSENGER and STB in year 2011; (f) MC6 observed by STB and Juno in year 2012; (g) MC7 observed by STA and Juno in year 2012; (h) MC8 observed by Wind and Juno in year 2013; (i) MC9 observed by MESSENGER and ACE in year 2014. The panels in each plot show the total field strength and the components (B_ϕ and B_z) in the MVA coordinate system. The x-axis presents the normalized time, in which 0 means the MC start and 1 means the end time.

parameters (r_0 and t_0) are the estimated radius and expansion time resulting from the V_p profiles. In this example, $t_{01} \approx 74$ hr with $r_{01} \approx 0.139$ au, and $t_{02} \approx 174$ hr with $r_{02} \approx 0.283$ au. The IPs are small at both spacecraft. Therefore, the observed velocity profiles are close to the distributions across the center. The difference obtained from the two V_p fits is $\Delta t_0 = t_{02} - t_{01} = 100$ hr, which is comparable to, but slightly shorter than, the observed time difference ($\Delta t = 122.5$ hr). This validates using this fitting model. It shows that, to first order, the change in the slope of the velocity profile within the MC

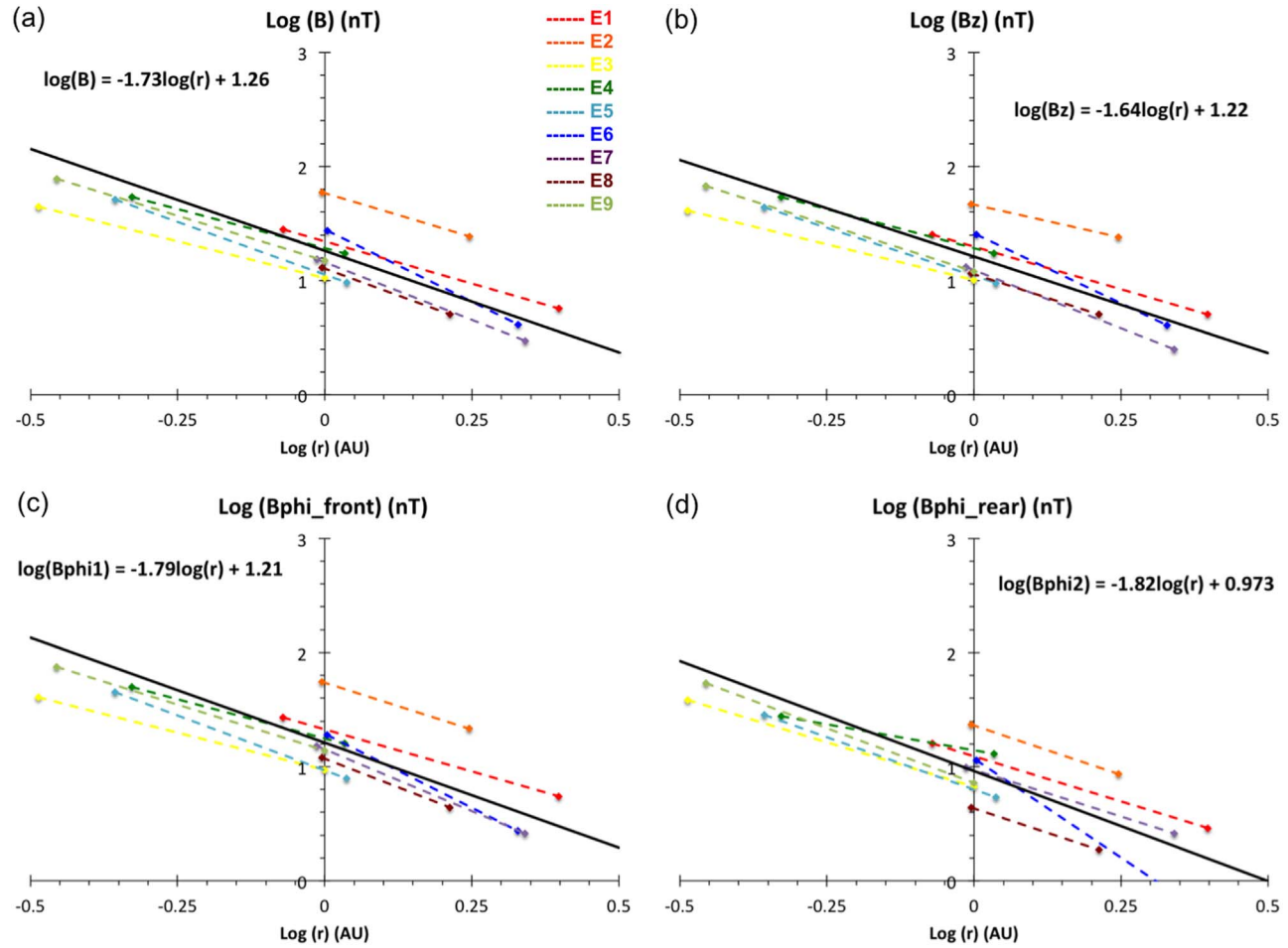

Figure 2. The distributions of the magnetic field strength and components with the distance away from the Sun. (a) Distributions of log(B) vs. log(r) of the nine MCs; (b) distributions of log(B_z) vs. log(r); (c) distributions of log($B_{\phi\text{front}}$) vs. log(r); (d) distributions of log($B_{\phi\text{rear}}$) vs. log(r). The black lines are the average of the linear fittings of the nine MCs' distributions, and the equations are shown in the panels.

can be understood from the expansion of the MC. This is the case even though these measurements occurred more than 5 days apart. If the difference of 22 hr between these two numbers is real, it may be because this MC experiences other forces (i.e., the interaction with the surrounding solar wind) that slow it down, in addition to expanding self-similarly. The difference may also reflect the influence of aging over the course of the measurements.

3.2. MC2—Measured by MESSENGER and STEREO-B on 2010 September 5–9

The second MC (E4) was observed by MESSENGER and STEREO-B (STB) in 2010 (MESSENGER: 2010-11-05T16:30:00–2010-11-06T14:00:00; STB: 2010-11-08T03:00:00–2010-11-09T09:00:00). MESSENGER was at 0.47 au, while STB was at 1.08 au. The longitudinal separation between the two SCs' positions is less than 1°. This event was previously studied in T. M. Salman et al. (2020). The ratios of eigenvalues from the MVA at the two SCs are 12.7 and 43.2. The large ratios indicate that this MC has clear magnetic field rotations, which can be seen in Figure 1(d). The orientations obtained from MVA show that the longitude separation of these two axes is ∼18°, and their latitude separation is ∼24°, which shows relatively good consistency. The duration of this MC increases from 21.5 hr at SC1 to 30 hr at SC2.

The B_{total} of SC1 shows a peak value close to the front boundary. But the B_{total} at SC2 is flatter and more symmetric. The magnetic field components at SC2 are more symmetric than at SC1. At SC2, the absolute value of B_ϕ at the rear boundary is close to the value at the front boundary, while B_ϕ at the rear boundary is just half of the value at the front boundary at SC1. In this event, $\gamma_{\text{front}} = 0.913$, which indicates that, globally, the axial and azimuthal magnetic fields decrease isotropically, while $\gamma_{\text{rear}} = 0.565$ shows that the local expansion is anisotropic and the axial field decreases faster than the azimuthal field (the expansion in B_z is faster than B_ϕ). This yields a flattening of the temporal profile of the magnetic field strength. The hump at the back of the B profile (blue) may be due to compression from a trailing faster stream. The resulting force imposed from outside would stop the expansion from being self-similar.

There are no velocity data at the MESSENGER spacecraft during the observation time. The velocity profile at the second spacecraft (STB) is presented in Figure 4(b). In this example, the velocity at STB decreases a little during the first half and increases in the second half ($\Delta V \sim -40\ \text{km s}^{-1}$), which shows that this MC is being compressed at the rear. This compression makes the rear part of the B_ϕ at SC2 different from SC1. It is also one of the reasons that γ_{rear} is much smaller than γ_{front} (0.913).

Table 2
Fitting Results of the Three Case Study Examples

Parameters	Helios 1	Voyager 2	MES	STB	Wind	Juno
$\theta - F$	52.6	28.2	−59.9	−33.7	71.9	65.9
$\theta - V$	54.1	28	−60.7	−34	69.2	65.7
$\phi - F$	299	302	288	254	317	320
$\phi - V$	299	307	288	252	328	324
$IP - F$	0.036	0.251	0.126	0.233	0.603	0.532
$IP - V$	0.038	0.323	0.131	0.262	0.659	0.559
$R - F$	0.151	0.252	0.103	0.144	0.16	0.204
$R - V$	0.151	0.247	0.103	0.144	0.166	0.207
$B_0 - F$	36.5	7.15	55.3	22.3	15.4	6.24
$B_0 - V$	38.5	7.8	56.7	23.1	17.4	6.68
$H - F$	+	+	−	−	+	+
$H - V$	+	+	−	−	+	+
$\alpha \times R/\tau - F$	1.9	1.89	2	2.37	1.49	1.44
$\alpha \times R/\tau - V$	1.97	1.98	2.04	2.4	1.64	1.54
$t_0 - F$	73.7	174	167	225	81.6	139
$t_0 - V$	73.7	174	167	225	81.6	139
$\chi^2 - F$	0.049	0.1	0.112	0.063	0.06	0.048
$\chi^2 - V$	0.05	0.087	0.102	0.068	0.046	0.04
$\chi^2_{B_{\rm total}} - F$	0.022	0.009	0.031	0.026	0.009	0.0024
$\chi^2_{B_{\rm total}} - V$	0.017	0.011	0.027	0.032	0.005	0.0015
$\chi^2_{B_{\rm total1}} - F$	0.097	0.086	0.446	0.063	0.048	0.002
$\chi^2_{B_{\rm total1}} - V$	0.089	0.07	0.457	0.054	0.068	0.003
$\chi^2_{B_{\rm total2}} - F$	0.212	0.007	0.04	0.068	0.029	0.004
$\chi^2_{B_{\rm total2}} - V$	0.015	0.006	0.008	0.111	0.003	0.001

Note. In the table, "F" indicates the fitting results obtained from C. J. Farrugia et al.'s (1992) radially expanding Lundquist solution, while "V" indicates the results from H. Shimazu & M. Vandas's (2002) isotropically expanding Lundquist model. From top to bottom, we present the orientations of the axis of the flux rope (θ and ϕ; degrees), the IP, the radius (R; au), the magnetic field magnitude at the axis (B_0; nT), the helicity (H, ±1), $\alpha \times R/\tau$ at the rear boundary, the expansion time before the MC encounters the SC (t_0; hr), the normalized chi-square of the three $\boldsymbol{B}$ components (χ^2), the normalized chi-square of the total magnetic field ($\chi^2_{B_{\rm total}}$), and the separate normalized chi-square values of the two parts of the MC (divided by the peak of the $B_{\rm total}$).

The fitting results are presented in Figure 4. The panels are the same as in Figure 3. The fittings at SC1 are better than at SC2. Both fittings on the magnetic field components are good, but the total magnetic field strengths show big differences between observations and fittings. The fittings at the front-half part are very similar by using these two expanding Lundquist solutions, while the fittings at the rear-half part usually show differences with these two solutions (see also the clearly different $\chi^2_{B_{\rm total2}}$ values obtained from the two solutions). In the fittings at SC1, the isotropic expansion solution fits the rear-half part better, while at SC2, the radial expansion solution fits better. This maybe so because with the compression at SC2, the local expansion of the MC transforms from being isotropic to radial. Therefore, this MC undergoes global isotropic expansion, and the local expansion is isotropic at SC1 and transforms to radial expansion at SC2.

3.3. MC3—Observed by Wind and Juno on 2013 April 14–18

The third MC (E8) was measured by Wind and Juno in 2013 (Wind: 2013-04-14T16:30:00–2013-04-15T18:00:00; Juno: 2013-04-17T01:30:00–2013-04-18T13:00:00). The longitude separation of the spacecraft is ∼1°. These SCs are radially aligned, with Wind at 0.99 au and Juno at 1.63 au. We apply the MVA on the magnetic field components and arrive at the orientations of the axes. The longitude difference is ∼21°, and the latitude difference is ∼6°. The magnetic field and its components in the MVA coordinate system are presented in Figure 1(h). We observe that the peak of the magnetic field magnitude at first SC is very close to the front boundary of the MC, and at the second SC farther away from the Sun, the peak has shifted toward the center. The rotations of the magnetic field at the two SCs are very similar. We calculate that $\gamma_{\rm front} = 1.26$, which indicates that the MC does not undergo a global isotropic expansion. And $\gamma_{\rm rear} = 0.932$ shows that the local expansion there tends to be isotropic.

We fit the V_p profile observed by SC1 and obtain $t_{01} = 81.6$ hr. For SC2, we do not have a velocity profile, and the time difference between the two observations is ∼57 hr. We thus estimate $t_{02} = 138.6$ hr. We input t_{01} and t_{02} into the radial self-similar expanding Lundquist model and isotropic self-similar expanding model and fit the three observed magnetic field components (in the GSE or RTN coordinate system). The fitting results of the third event are presented in Figure 5. Both fittings at the two SCs are good, especially at the second SC. In

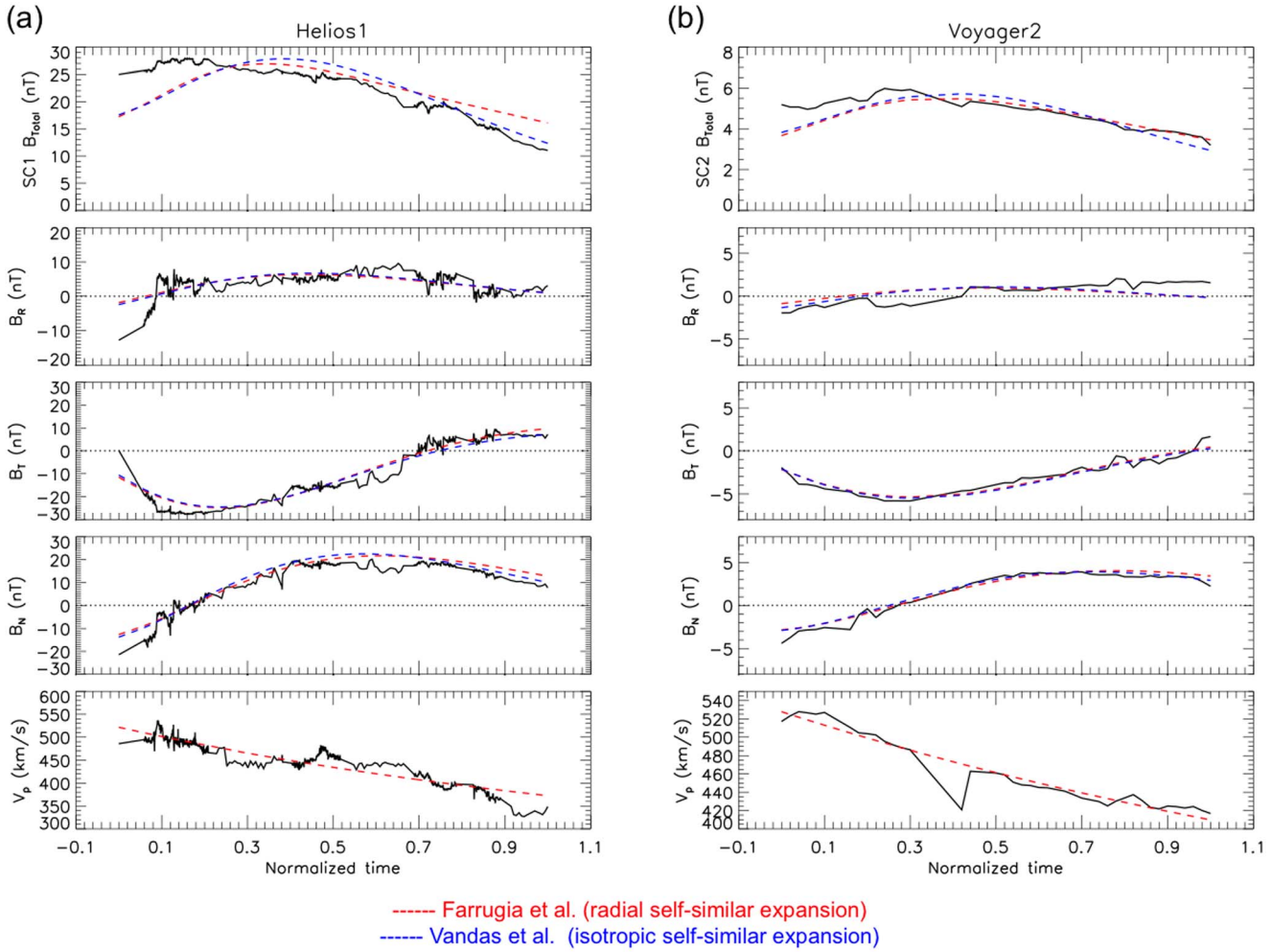

Figure 3. The fittings of the MC observed by Helios 1 and Voyager 2 in the year 1978. Helios 1: 1978-03-02T00:00:00–1978-03-03T05:45:00; Voyager 2: 1978-03-07T02:30:00–1978-03-09T04:00:00. The panels are the total $\boldsymbol{B}$ (black, observed; red, radial self-similar expansion solution; blue, isotropic self-similar expansion solution; nT), three B components in the RTN coordinate system (nT), and proton velocities (black, observed data; red, linear fitting of V_p; km s^{-1}).

this MC, at the front-half part, the radial expansion model fits better, while at the rear-half part, the isotropic expansion model fits better. This result is consistent with the γ values. Since $\gamma_{\rm front}$ shows the front-half part and its value suggests that the global expansion is not necessarily isotropic, the fittings at the front-half part prove this result (the radial expansion solution is better). $\gamma_{\rm rear}$ shows the rear-half part, and the value suggests a local expansion that is likely isotropic (the fitting also shows that the isotropic expansion solution is better).

4. Results and Discussion

In this work, we study nine MCs, each measured in situ by two SC separated by more than 0.5 au. We investigate how the axial and azimuthal magnetic field components decay as the MC propagates away from the Sun. We focus on finding out whether the MCs expand self-similarly in the solar wind or not. By analyzing how the maximum magnetic field strength decreases with heliospheric distance, we find that the MCs expand self-similarly (the magnitudes of $\boldsymbol{B}$ and its components decrease in order of distance). For these nine events, the maximum magnetic field strength as a function of r is of the form $B_{\rm max} \propto r^{-1.73\pm0.39}$. The expansion rates of these MCs are faster than E. E. Davies et al.'s (2022) results, $B_{\rm mean(\leqslant 1\ au)} \propto r^{-1.49\pm1.12}$ and $B_{\rm mean(\geqslant 1\ au)} \propto r^{-1.29\pm0.83}$, but comparable to other past studies (Y. Liu et al. 2005; T. M. Salman et al. 2020).

Further, we focus on determining whether the axial and azimuthal magnetic field components decrease at the same rate (isotropic expansion) or not (anisotropic expansion). To the best of our knowledge, this is one of the first studies investigating this particular aspect of MC evolution. We find that the azimuthal component (B_ϕ) is decreasing faster than the axial component (B_z), and that the decrease of the azimuthal component at the back half is even faster. B_z has a -1.64 ± 0.405 index, which is consistent with the results from M. Leitner et al. (2007), who obtained an index of -1.64 over modeled values, whereas B_ϕ has -1.79 ± 0.424 and -1.82 ± 0.687 indexes at the front and rear boundaries, respectively (see Figure 2).

The global and local expansions are not always consistent with each other (N. Lugaz et al. 2020). This conclusion is supported by the different indices reported above. From the three MC examples we discussed in detail, we find that the fitting of the rear-half part of the MC is better than that of the front-half part. Since the rear-half part of the MC is affected by the local expansion more than the front-half part, we can treat the two parts of the MC separately when we do the fitting. The reconstruction of the front-half part could provide us

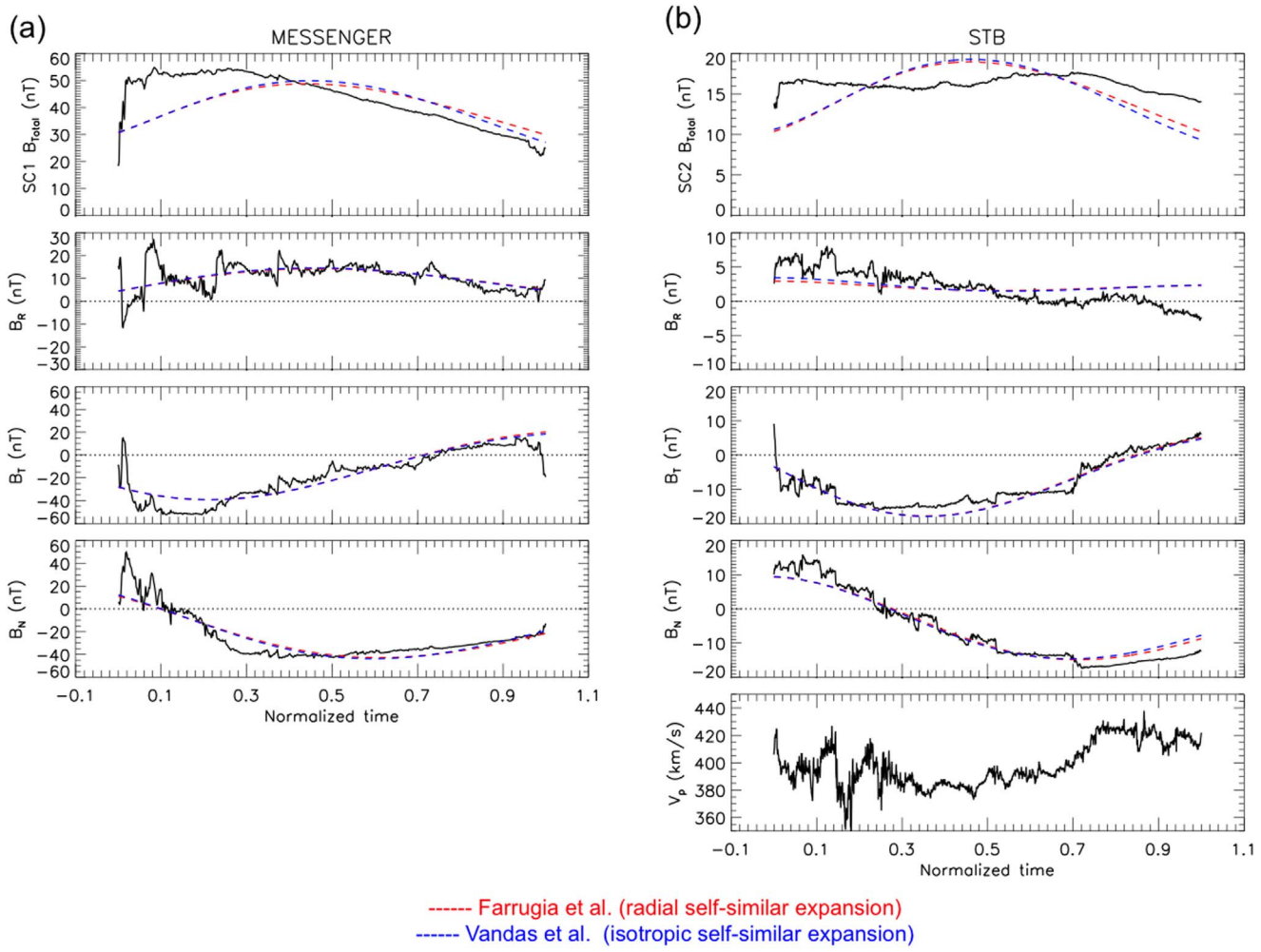

Figure 4. The fitting of the MC observed by MESSENGER and STB in the year 2010. MESSENGER: 2010-11-05T16:30:00–2010-11-06T14:00:00; STB: 2010-11-08T03:00:00–2010-11-09T09:00:00. The panels are the same as the first example. There are no V_p data at the MESSENGER spacecraft.

information about the global expansion, while the fitting results on the rear-half part are more related to the local expansion of the MCs.

Considering the different expansion rates of the magnetic field components with heliospheric distance, we find a simple way to check if an MC undergoes self-similar expansion and whether the self-similar expansion is radial or isotropic and therefore judge if the global expansion or local expansion are consistent or not. We introduce a parameter γ, which is calculated by using the magnetic field measurements obtained by two distant spacecraft. We use the MVA method on the observed magnetic fields and transfer the data into the MVA coordinate system, in which the rotations of the magnetic field components can be compared.

At the front-half part of the MC, the expansion velocity has the same direction as the solar wind velocity. Since the expansion velocity is typically much smaller than the solar wind speed, the expansion effect is not obvious there. Therefore, the $\gamma_{\rm front}$ value tells us more about the global expansion. The fitting results on the front-half part are usually similar, which indicates that the local expansion has less effect on this part's fitting. At the rear-half part of the MC, the expansion velocity has a different direction from the solar wind velocity. The expansion effect is more clear than at the front-half part. Then the $\gamma_{\rm rear}$ values tell us more about the local expansion effect. In this part's fitting, the local expansion affects the results more.

The decrease of B_ϕ is usually different at the two parts (front-half part and rear-half part). One reason may be that the determination of the rear-half part is not exact, which can directly affect the MVA results and therefore the γ distributions. How to define the boundary of the MC is always an important question but, as many studies have pointed out, not an easy one to solve.

We compare the value of γ with the distance between the measurements obtained by two spacecraft. For these nine events, we have five cases with $\gamma_{\rm front}$ between 0.8 and 1.2, and eight cases have $\gamma_{\rm front}$ between 0.7 and 1.3. This argues in favor of the evolution of these MCs being globally isotropically self-similar, in agreement with the analytical models of H. Shimazu & M. Vandas (2002) and D. B. Berdichevsky et al. (2003). In addition, six cases have $\gamma_{\rm front} > 1$, which indicates that the azimuthal component decreases faster in the front half of the MC. However, while most of the MC examples show that the global expansion tends to be isotropic, the local expansion usually presents an anisotropic expansion mode (only four cases have $\gamma_{\rm rear}$ between 0.8 and 1.2). As first pointed out by V. A. Osherovich et al. (1993), a flattening of the time profile of $B_{\rm total}$ develops farther from the Sun if the expansion is self-similar and radial. To visualize this, imagine a spacecraft

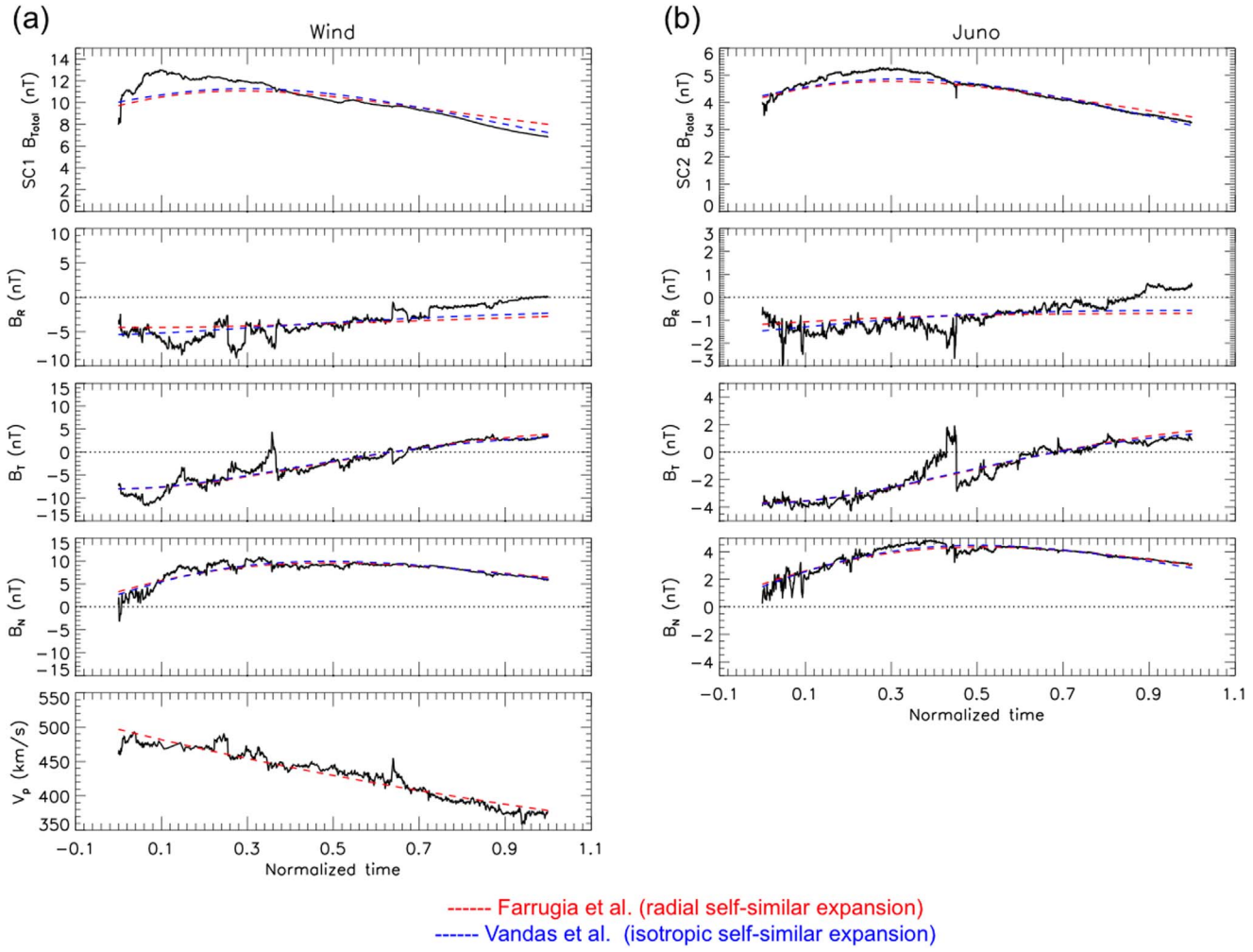

Figure 5. The fitting of the MC observed by Wind and Juno in the year 2013. Wind: 2013-04-14T16:30:00–2013-04-15T18:00:00; Juno: 2013-04-17T01:30:00–2013-04-18T13:00:00. The panels are the same as the first example. There are no V_p data at the Juno spacecraft.

whose trajectory passes through the cloud's axis and at right angles to it. The azimuthal component B_ϕ contributes mostly to the wings of the profile. Since B_ϕ decreases slower with time than the axial field B_z, the resulting effect is to flatten the profile as time passes.

In our study, we consider the MVA results as appropriate if the eigenvalue ratio (intermediate-to-minimum) is greater than 3. In these cases, the orientations of the axis are well determined if the IPs are low in the observations (N. Al-Haddad et al. 2013). However, the IP is not always small. The two spacecraft are not always crossing close to the center of the MC, so they might not observe the same portion of the MC. The limitations are impossible to overcome with today's observations. In addition, we require that all the events in this study should have clear rotations in the magnetic field components. This feature is not satisfied by all of the MCs. The conclusions in this study do not necessarily hold for all the conjunction events. Other factors, such as the ambient solar wind conditions (e.g., example 2), interaction with other structures in the heliosphere, and magnetic erosion, have also been shown to play important roles in shaping the evolution of the MC. One point is that the location of the peak $\boldsymbol{B}$ sometimes shifts from being close to the front boundary to being closer to the center at larger distances from the Sun. Assuming that the shift toward the leading edge of the MC is a result of expansion (V. A. Osherovich et al. 1993), this trend shows that, during propagation, the expansion is being affected by other factors. Thus, while long-distance quasi-radial conjunctions are of great value in determining the expansion mode, the long delay between observations may give time for other interactions with the solar wind to develop, such as collisions with faster streams. Therefore, predicting the exact evolution of an MC during propagation can still be a challenging task even with knowledge of its expansion mode.

Acknowledgments

All UNH authors acknowledge grant 80NSSC20K0431. W.Y., N.A., and F.R. acknowledge grants 80NSSC22K0349, 80NSSC21K0463, and AGS1954983. N.L. acknowledges additional support from 80NSSC20K0700. B.Z. acknowledges additional support from 80NSSC23K1057 and AGS-2301382. C.J.F. acknowledges support from grant 80NSSC21K0463 and Wind's grant 80NSSC19K1293. A.B.G. acknowledges support from grant STEREO 80NSSC20K0431.

ORCID iDs

Wenyuan Yu https://orcid.org/0000-0002-2917-5993
Nada Al-Haddad https://orcid.org/0000-0002-0973-2027
Charles J. Farrugia https://orcid.org/0000-0001-8780-0673

Noé Lugaz https://orcid.org/0000-0002-1890-6156
Bin Zhuang https://orcid.org/0000-0002-5996-0693
Florian Regnault https://orcid.org/0000-0002-4017-8415
Antoinette B. Galvin https://orcid.org/0000-0003-3752-5700

References

Al-Haddad, N., Nieves-Chinchilla, T., Savani, N. P., et al. 2013, SoPh, 284, 129
Berdichevsky, D. B., Farrugia, C. J., Lepping, R. P., et al. 2003, in AIP Conf. Ser. 679, Solar Wind Ten, ed. M. Velli et al. (Melville, NY: AIP), 758
Burlaga, L., Sittler, E., Mariani, F., & Schwenn, R. 1981, JGR, 86, 6673
Burlaga, L. F. 1988, JGR, 93, 7217
Cane, H. V., & Richardson, I. G. 2003, JGRA, 108, 1156
Chi, Y., Shen, C., Wang, Y., et al. 2016, SoPh, 291, 2419
Davies, E. E., Möstl, C., Owens, M. J., et al. 2021, A&A, 656, A2
Davies, E. E., Winslow, R. M., Scolini, C., et al. 2022, ApJ, 933, 127
Démoulin, P., & Dasso, S. 2009, A&A, 498, 551
Démoulin, P., Nakwacki, M. S., Dasso, S., & Mandrini, C. H. 2008, SoPh, 250, 347
Farrugia, C. J., Burlaga, L. F., Osherovich, V. A., & Lepping, R. P. 1992, in Proc. 3rd COSPAR Coll: Solar Wind Seven, ed. E. Marsch & R. Schwenn (Amsterdam: Elsevier), 611
Farrugia, C. J., Burlaga, L. F., Osherovich, V. A., et al. 1993, JGR, 98, 7621
Farrugia, C. J., Janoo, L., Torbert, R. B., et al. 1999, in AIP Conf. Proc. 471, The Solar Wind Nine Conf., ed. S. R. Habbal et al. (Melville, NY: AIP), 745
Gold, T., & Hoyle, F. 1960, MNRAS, 120, 89
Good, S. W., Kilpua, E. K. J., LaMoury, A. T., et al. 2019, JGRA, 124, 4960
Gulisano, A. M., Démoulin, P., Dasso, S., Ruiz, M. E., & Marsch, E. 2010, A&A, 509, A39
Hidalgo, M. A., Cid, C., Vinas, A. F., & Sequeiros, J. 2002, JGRA, 106, 1002
Klein, L. W., & Burlaga, L. F. 1982, JGR, 87, 613
Leitner, M., Farrugia, C. J., Möstl, C., et al. 2007, JGRA, 112, A06113
Lepping, R. P., Jones, J. A., & Burlaga, L. F. 1990, JGR, 95, 11957
Liu, Y., Richardson, J. D., & Belcher, J. W. 2005, P&SS, 53, 3
Lugaz, N., Salman, T. M., Winslow, R. M., et al. 2020, ApJ, 899, 119
Lundquist, S. 1950, Ark.fys, 2, 361
Mulligan, T., Russell, C. T., Anderson, B. J., & Acuna, M. H. 2001, GeoRL, 28, 4417
Osherovich, V. A., Farrugia, C. J., & Burlaga, L. F. 1993, AdSpR, 13, 57
Regnault, F., Al-Haddad, N., Lugaz, N., et al. 2023, ApJ, 957, 49
Regnault, F., Al-Haddad, N., Lugaz, N., et al. 2024, ApJ, 962, 190
Salman, T. M., Winslow, R. M., & Lugaz, N. 2020, JGRA, 125, e27084
Shimazu, H., & Vandas, M. 2002, EP&S, 54, 783
Sonnerup, B. U. Ö., & Scheible, M. 1998, ISSIR, 1, 185
Vršnak, B., Amerstorfer, T., Dumbović, M., et al. 2019, ApJ, 877, 77
Vršnak, B., Ruždjak, D., Sudar, D., & Gopalswamy, N. 2004, A&A, 423, 717
Wang, Y., Zhou, Z., Shen, C., Liu, R., & Wang, S. 2015, JGRA, 120, 1543
Wang, Y., Zhuang, B., Hu, Q., et al. 2016, JGRA, 121, 9316
Yu, W., Al-Haddad, N., Farrugia, C. J., et al. 2022, ApJ, 937, 86
Zhuang, B., Lugaz, N., Al-Haddad, N., et al. 2023, ApJ, 952, 7